RESEARCH ARTICLE

High-Sensitivity Wearable Sensors Based on Porous Graphene Belts for Human Motions Detection

SHUAI LIU AND ZHAOFA ZHANG

College of Textile Science and Engineering, Zhejiang Sci-Tech University, Hangzhou 310000, China

Corresponding author: Zhaofa Zhang (zhaofazhang@zstu.edu.cn)

ABSTRACT Sensing and responding to human motion stimuli are important features of wearable electronic devices. The design and construction of deformable inner structures increase wearable sensors' sensitivity and accuracy. In this study, reduced graphene oxide porous belts (rGO-PBs) were successfully designed and prepared using the intercalation/reduction method. The linear belts had excellent flexibility and conductivity. Then, the flexible rGO-PBs were encapsulated with PDMS to construct wearable sensors. The rGO-PB sensors demonstrated excellent accuracy, a fast response time (about 75 ms), a large sensing range (0-180°), and outstanding durability (4,000 cycles). With these excellent properties, the belt-based wearable sensors could monitor human motions, such as large joint movements and subtle muscle vibrations, detect voices, and identify sample words. This outstanding performance indicated that the prepared rGO-PBs have numerous possibilities for application in wearable electronic devices.

INDEX TERMS Deformation sensing, porous structure, wearable sensor, linear belt.

I. INTRODUCTION

Graphene has excellent force, thermal, optical, and electrical properties and many application prospects [1], [2], [3], [4]. The layered structure of graphene nanoscale flakes is easy to stack and forms a membrane. These properties give it high electron mobility and tensile strength, and it can be used as raw materials for energy storage devices [5], [6] and sensors [7], [8], [9]. With the development of electronic skin and people's improved quality of life, more accurate, efficient, portable health and exercise monitoring sensors are demanded [10], [11], [12], [13]. Flexible and wearable sensors [14], [15], unlike traditional sensors, can be directly worn on a person's skin and realize the real-time monitoring of physiological activities [16], [17], [18], [19]. Among these sensors, graphene-based sensors

have higher sensitivity and flexibility and can quickly detect subtle changes in human movements [20], [21], [22]. Nowadays, graphene is usually used as a conductive material to construct one-dimensional (1D) fiber or yarn sensors [23], [24], two-dimensional (2D) film or fabric sensors [20], [25], or three-dimensional (3D) aerogel sensors [26]. Since the special conjugated electronic structure and strong van der Waals force, it is easy to stack and form 2D graphene films. Nowadays, graphene and graphene oxide (GO) have been utilized as the raw materials for the fabrication of graphene films [27], [28]. Compared with graphene, GO with oxygen-containing functional groups, can be formed into stable colloidal suspension. This property is beneficial for the formation of laminated and highly oriented structures. Followed by the reduction process, the reduced graphene has controllable structural and chemical properties, making it one of the most important precursors for fabricating graphene films.

The associate editor coordinating the review of this manuscript and approving it for publication was Yogendra Kumar Prajapati.

Graphene-based porous materials usually include 2D porous films and 3D porous aerogels [29]. 2D porous graphene-based films usually refer to holey graphene or graphene nano-mesh. As previously reported researches, these 2D porous graphene films possess abundant micro- to meso-holes or pores, using for filtering or molecular screening [30]. In addition, 3D porous graphene-based materials include graphene aerogel, graphene foam, and graphene sponge [31]. These porous graphene-based materials are prepared by self-assembly or template assisted method. The porous templates, such as like metal oxides [32], commercial Ni foams [33],or nickel NPs [34] are used to construct porous structures. The applied template was then removed, leading to the production of 3D porous graphene.

However, designing graphene-based 2D porous materials is still challenging. The large-scale production of graphene-based porous materials is also difficult [35], [36]. The design and construction of these materials with a deformable inner structure is an effective way to improve their sensing performance [37]. Recently, Jia et al. used a pre-stretching method to generate wrinkles and improve the performance of sensors. The prepared graphene film-based pressure sensor had an outstanding sensitivity, reaching $178\ kPa^{-1}$ [38]. Sheng et al. used a GO aqueous dispersion to form a porous structure to prepare pressure sensors, which demonstrated a high sensitivity of $161\ kPa^{-1}$ [39]. But using carbonate particles as a template, to construct 2D porous graphene films still lacks research. In addition, using the reduction method to prepare porous graphene films proved to be a feasible method [40], [41], which graphene oxide films (GO-Fs) were used as raw materials. Materials with porous [42], [43], wrinkled structures, or rough surfaces have deformable inner structures, and they are feasible to design. These deformable structures could enhance the signal accuracy, and facilitate and improve the performance of sensors. Constructing porous structures can effectively improve the deformation sensing performance and conductivity of graphene-based materials, and also expand their applications.

In order to improve the wearability and sensing performance, a facile and simple method used to form porous graphene belts is presented in this paper. The preparation method is simple and reproducible. The porous structures were successfully designed and prepared using the intercalation/reduction method. The porous structures endow excellent electrical and flexible properties to the belts. Meanwhile, the porous belts demonstrated good performance and sensitivity in detecting bending degrees. The prepared belts were used to fabricate wearable sensors. The porous graphene belt sensors demonstrated excellent flexibility, accuracy, a fast response time, and durability in detecting human motions. In this study, the prepared sensor demonstrated a proof-of-concept and will be finalized for wearable sensors. The prepared wearable sensors based on porous graphene belts would have good application prospects in detecting various human motions.

II. MATERIALS AND METHODS
A. RAW MATERIALS
Graphene oxide aqueous dispersion (GO, 10mg/mL, Carbon Fountain Technology), anhydrous sodium carbonate (Na_2CO_3, $\geq$99wt%, Yungtay Chemical Reagent Co., Ltd.), hydriodic acid (HI, AR, $\geq$47.0%, Meeker Chemical Co., Ltd.), and polydimethylsiloxane (a 10:1 mixture of prepolymers and curing agents, Sylgrad-184, Dow Corning) were acquired and used as received.

B. PREPARATION OF REDUCED GRAPHENE OXIDE POROUS BELTS (rGO-PBs)
Firstly, Na_2CO_3 solutions with different concentrations (0.2-1 mol/mL) were prepared. Then, 1 mL salt solution was taken and mixed with 9 mL GO solution (7 mg/mL) to prepare the composited solution at room temperature for 1 hour. The composited solution was thoroughly stirred to obtain a uniformly mixed GO solution. 9 mL of the blended solution was transferred into a 3×10 cm polystyrene mold. The mixed solution was dried in an oven at $60\,^{\circ}C$ for 12 hours. After that, a graphene oxide film (GO-F) containing Na_2CO_3 particles was obtained. The composited GO-Fs were reduced at $200\,^{\circ}C$ for 8 hours using HI for chemical reduction. After reduction, the membrane was repeatedly sonicated and washed in anhydrous ethanol. After drying, a reduced graphene oxide porous film (rGO-PF) was obtained. The prepared film was cut into linear reduced graphene oxide porous belts (rGO-PBs) using a roller blade. For comparison, the pure graphene oxide films (GO-Fs) and reduced graphene oxide belts (rGO-Bs) were also prepared by the same preparing method as above mentioned. For clarity, graphene oxide film was defined as GO-F, reduced graphene oxide film was defined as rGO-F, reduced graphene oxide belt was defined as rGO-B, reduced graphene oxide porous film was defined as rGO-PF, reduced graphene oxide porous belt was defined as rGO-PB.

C. CONSTRUCTION OF rGO-PB SENSORS
The prepared rGO-PB was used as a conductive core material. Both ends of the rGO-PB were connected to conductive copper belts. Then, PDMS was used as a protective and insulative film. The encapsulated rGO-PB sensors were dried at $80\,^{\circ}C$ for 8 hours. The prepared wearable sensors were attached to a person's finger, wrist, arm, and throat. The medical-grade double-sided adhesive was utilized to adhere the sensor to the surface of the skin. Sensing signals were detected using a Keithley Ke2400s digital source meter.

D. CHARACTERIZATION
The morphologies of prepared samples were observed and tested via EDS using a field thermal emission scanning electron microscope (vltra55), and the resistance changes were measured with a Keithley Ke2400s digital source meter (output current 0.001mA). The mechanical properties of the rGO-PBs were measured with an Electronic Textile strength

instrument (YG026T-II, Ningbo Textile Instrument Factory, China). N_2 adsorption tests for specific surface areas were conducted using the fully automated surface area and porosity analyzer (Micromeritics ASAP 2460). The X-ray powder diffraction (XRD) data were done using X-Ray Diffractometer (BRUKER D8 Advance). The FTIR spectra of prepared samples were tested with FTIR analyzer (Nicolet 5700). The XPS (K-Alpha)was also used to characterized the prepared samples.

III. RESULTS AND DISCUSSION

A. PREPARATION AND INNER STRUCTURE OF rGO-PBs

The porous belts are prepared as illustrated in Figure 1. Firstly, different mass proportions of reduced graphene oxide porous films (rGO-PFs) were designed and prepared as shown in Figure 1(a). The produced films formed an ununiform porous structure between the layers, as illustrated in Figure 1(a). The membrane was easily cut into linear belts. Compared to the rGO-PFs, the porous belts with a linear structure were highly flexible. The linear belts were encapsulated with PDMS to form wearable sensors, as shown in Figure 1(a). The flexible rGO-PB sensors were used to monitor large joint and muscle movements and tiny vibrations, as demonstrated in Figure 1(b).

FIGURE 2. Morphologies of rGO-PBs and their chemical and physical properties. (a) SEM images of composited GO-F and rGO-PBs; (b) Morphology and preparation principle of rGO-PBs (1-the cross-section image of composited GO-F (Na_2CO_3 particles marked with red dashed circles), 2-the cross-section image of rGO-PB, 3-the enlarged image of inner pores of rGO-PB, 4-schematic diagram of the preparation process of rGO-PB); (c) elemental analysis of rGO-PBs before and after reduction; (d) specific surface areas of graphene belt and rGO-PBs at different concentrations (from 0.2 to 1 mol/mL); (e) stress–strain curves of pure rGO-B and rGO-PBs at different concentrations.
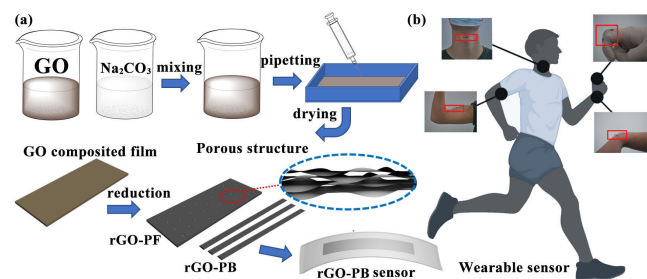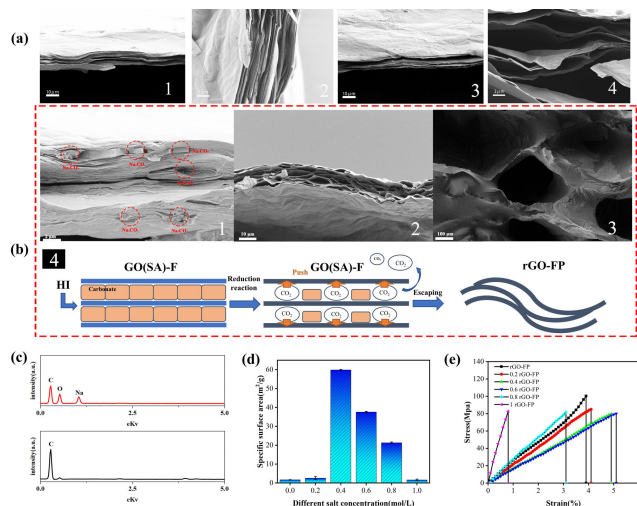

FIGURE 1. Preparation of rGO-PBs and their application. (a) Illustration of design and formation of rGO-PBs; (b) rGO-PB sensors used to monitor human motions.

The morphology and inner structure of the prepared composited GO-Fs and rGO-PBs are observed and shown in Figure 2. A cross-section SEM image of the composited GO-F showed a typical lamellar structure, as shown in Figure 2(a)-1. The thickness of the composited film was about 5 μm. It can be seen that the composited GO-Fs showed typical lamellar structures. The partially enlarged composited GO-F is shown in Figure 2(a)-2. Na_2CO_3 particles were present between the compressed lamellar structures. The inner structure of the rGO-PBs can be observed in Figure 2(a)-3. The rGO-PBs also demonstrated a lamellar structure. The thickness of rGO-PB was about 8 μm, which was larger than that of the composited GO-F. However, the rGO-PBs had porous inner structures, as the partially enlarged figure shown in Figure 2(a)-4. The porous structure formed during the reduction process. For comparison, a pure reduced graphene oxide belt (rGO-B) is also observed in the Supplementary Materials (Figure S1). This pure rGO-B

demonstrated a neat layer-upon-layer structure, showing a typical feature of graphene film [44], [45]. Unlike the layer stacking structure of pure graphene film and composited GO-Fs, a large gap was present between the graphene layers of each rGO-PB. When received external stimuli, this inner porous structure would facilitate deformation sensing and cause resistance changes, as illustrated in Figure 1(a). The interfacial interactions among the rGO-PBs and the distribution morphology of salt particles inside the membrane were also analyzed. The Na_2CO_3 particles marked with red dashed circles intercalated between the GO layers as the cross-section image shown in Figure 2(b)-1. Since the uneven sizes of salt particles, the rGO-PBs formed nonuniform pores as shown in Figure 2(b)-2. The irregular pores horizontally distributed along the membrane as shown in Figure 2(b)-2. More importantly, the outer shell above and below the porous film was intact, providing continuous support for subsequent sensing. Furthermore, the enlarged view of pores also confirmed the inner porous structure of rGO-PBs after the reduction process as demonstrated in 2(b)-3. These special structures would provide the possibility for rGO-PBs to possess outstanding sensing performance.

The mechanism of forming rGO-PBs is illustrated in Figure 2(b)-4. In the initial state, Na_2CO_3 particles were mixed into and layered between the GO sheets. During the formation of the film, the GO sheets were reconstructed and stacked layer by layer. Meanwhile, the Na_2CO_3 particles also accumulated as the interlayer water evaporated. And the Na_2CO_3 particles were stacked and enclosed within the lamellar flakes structure as illustrated in Figure 2(b)-1.

The Na_2CO_3 particles intercalated between the GO layers and worked as templates for forming pores. The composited GO-F had a neat, layer-upon-layer structure as shown in Figure 2(a)-1. Then, the reduction process subsequently continued. During the reduction process, the oxygen-containing functional groups of GO were reduced by HI. Meanwhile, HI also reacted with the Na_2CO_3 particles. A compound reaction occurred between the carbonate and acid during the reduction process. The Na_2CO_3 particles underwent double decomposition and turned into an ionic state. The original positions of Na_2CO_3 particles would change into holes as shown in Figure 2(b)-2. More importantly, CO_3^{-2} produced CO_2, expanding the original size of the pores. The interlayer CO_2 gas enlarged the interlayer spacing during the escape of CO_2. The intercalated salt particles and the effect of CO_2 gas created numerous holes between the lamellar structure. These pores were irregularly distributed between the flakes and greatly increased the specific surface area of the rGO-PBs as demonstrated in Figure 2(b)-2 and -3. After reduction, all the salt ions were washed away, and the rGO-PBs were finally obtained.

The elemental analysis of composited GO-F and rGO-PBs was also performed using EDS, as shown in Figure 2(c). The results show that the composited GO-F mainly consisted of three elements: C, O, and Na. These results indicated the Na_2CO_3 particles were inserted between the GO sheets. After reduction, the rGO-PBs only contained C and O elements. The peak intensity of the O element was obviously decreased after reduction. These results were caused by that the oxygen-containing functional groups of GO were reduced with HI. The carbonate and acid ions underwent a double-decomposition reaction and were washed away. These results show that the oxygen-containing functional groups were reduced, and the Na_2CO_3 particles were almost removed. The XRD was also used to characterize the chemical properties of the prepared rGO-B and rGO-PB. The XRD patterns of pure GO-F, rGO-B, composited GO-F (containing Na_2CO_3 particles), and rGO-PB are shown in Figure S2 (Supplementary Materials). The diffraction peak is observed at 10.9° for GO-F, attributed to the introduction of oxygen-containing functional groups [46]. After reduction, rGO-B exhibited a distinct diffraction peak at 24.3°, indicating the removal of oxygen-containing groups [47]. And the diffraction peak at 10.9° disappears completely indicating the development of a certain graphitic structure. A broad band at about 25° appeared in the XRD pattern of composited GO-F (containing Na_2CO_3 particles), indicating that Na_2CO_3 particles inserted between GO sheets. And the slight reduction of GO in the forming process since Na_2CO_3 can be used as a reduction agent at high temperatures [48]. After reduction, the peak of rGO-PB obviously became broad, indicating a disorder in internal structure since its inner porous structure. In addition, the prepared GO-F, composited GO-F, and rGO-PB were analyzed by FTIR as shown in Figure S3. The main functional groups were recognized, such as epoxy

(1039 cm^{-1}, -O- stretching), hydroxyl (1390 cm^{-1}, -OH deformation), carboxyl or carbonyl (1614 cm^{-1}, -OH stretching and 1720 cm^{-1}, C=O stretching) [49]. Compared to GO-F, the peak intensity at 3425 cm^{-1} of the carboxylic acid or alcohol groups decreased and the peak at 1720 cm^{-1} diminished, indicating the carboxyl groups of the composited GO-F were decomposed since the slight reduction. The peak at 705 cm^{-1} was the carbonate bands of Na_2CO_3. After reduction, the peaks at 1039 cm^{-1} and 1390 cm^{-1} were also decomposed indicating the GO was reduced to rGO [50]. Meanwhile, the peak at 705 cm^{-1} decomposed indicated the Na_2CO_3 particles underwent double decomposition [51]. Furthermore, XPS was also used to characterize the prepared samples. The GO-F only contained C and O elements, as the C1s (284.1 eV) and O1s (532.1 eV) peaks are shown in Figure S4. Na1s peak (1072.1 eV) could be seen in the composited GO-F as demonstrated in Figure S4. After reduction, the rGO-PB only had C and O elements, indicating the Na_2CO_3 particles were reacted and removed since the double decomposition reaction. Compared to GO-F and composited GO-F, the intensity of O1s was decreased, indicating the Oxygen-containing functional groups of GO were reduced. And the results corresponded to XRD analyses. Through the characterization of EDS, XRD, and FTIR, the oxygen-containing functional groups of GO were reduced by HI. And the Na_2CO_3 particles underwent double decomposition during the reduction process. These results proved that the rGO-PBs were prepared after reduction.

The specific surface area is an important feature of porous materials. The specific surface areas are shown in Figure 2(d). The specific surface area was different since the concentrations of Na_2CO_3 solution ranged from 0 to 1 mol/L. The specific surface area of pure rGO-B was 1.65 m^2/g. The specific surface area of rGO-PBs showed an increasing and then decreasing trend with an increasing salt concentration. The maximum value of the specific surface area of rGO-PBs was 59.83 m^2/g when the salt concentration of 0.4 mol/L. It is not difficult to understand that the increasing trend of the specific surface area of rGO-PBs from 0 to 0.4 mol/L. The results were caused by salt particles occupying the interlayers and forming porous structures during the reduction process. As the salt concentration increased, the pore space increased, and thus the specific surface area effectively increased. But as the concentration of salt increased from 0.6 to 1 mol/L, more Na_2CO_3 particles accumulated and seriously affected the layer structure. The inner structure showed an obvious agglomeration phenomenon at a concentration of 1 mol/L. The SEM image of the composited GO film is shown in Figure S5. The Na_2CO_3 particle occurred serious accumulation. After reduction, the film became fractured, seriously damaging its mechanical properties. And the salt particles not only intercalated between the layer structure, but also appeared on the surface. These phenomena destroyed the layered structure of the rGO-PBs. These events also led to a decrease in the porosity, and thus a gradual decrease in

the specific surface area. Moreover, the inner structure also showed an obvious agglomeration phenomenon at a concentration greater than 1 mol/L. This agglomeration phenomenon resulted in the structure of the rGO-PBs becoming fragile. A higher concentration would have led to an unstable rGO-PB structure, making them difficult to use as sensor materials.

The mechanical properties of the rGO-PBs are also analyzed and shown in Figure 2(e). The breaking strength gradually decreased with the increase in salt concentration, as shown in Figure 2e. The pure graphene belts had a max tensile stress of 100.3 MPa. The tensile strength of the rGO-PBs decreased due to the increase in salt concentration. However, the breaking elongation of the rGO-PBs demonstrated first increased, and then decreased. The rGO-PBs had a max strain of 5.1% at a concentration of 0.6. And the elongation at break of rGO-PBs was 4.9% at the concentration of 0.4. The breaking strengths of the rGO-PBs were about 79.5 MPa and 80 MPa at salt concentrations of 0.4 and 0.6, respectively. The porous structure increased the layer space and led to the tensile strength decreasing. The rGO-PBs had a larger specific surface area at a concentration of 0.4, showing an excellent and stable porous structure. The porous structure increased the number of wrinkles in the inner structure, leading to more space and deformation. After analyzing the specific surface area and mechanical properties, the rGO-PBs at a concentration of 0.4 were chosen as the raw material used to construct wearable sensors.

B. PERFORMANCE OF rGO-PB SENSOR

In order to analyze the sensing performance, pure rGO-Fs were also cut into belts (rGO-Bs). The resistance changes in the rGO-Bs and rGO-PBs under different bending angles were analyzed and shown in Figure 3. The resistance changes in the pure rGO-Bs under different bending angles are shown in Figure 3(a). The resistance changes curves of the rGO-Bs demonstrated a stepwise trend at bending degrees from 30° to 120°, reflecting the characteristics of deformation sensing. In the range from 120° to 180°, the resistance of the rGO-Bs was almost unchanged. These results probably resulted from the larger bending angles affecting the inner structure. At a bending degree of 120°, the inner graphene nanosheets almost underwent the largest deformation. Further bending could not cause its inner structural changes.

The gauge factor (GF) is an important factor in evaluating the performance of sensors. In this paper, the GF was calculated as follows [52]:

$$GF = \frac{\Delta R}{R\Delta\varepsilon} \quad (1)$$

$$\varepsilon = \frac{h}{2r} \quad (2)$$

$$c = 2r \times \sin\left(\frac{I}{2r}\right) \quad (3)$$

In the equation above, R represents the initial resistance, ΔR represents the resistance variation, ε represents tensile strain, h represents the sensor thickness, r represents the
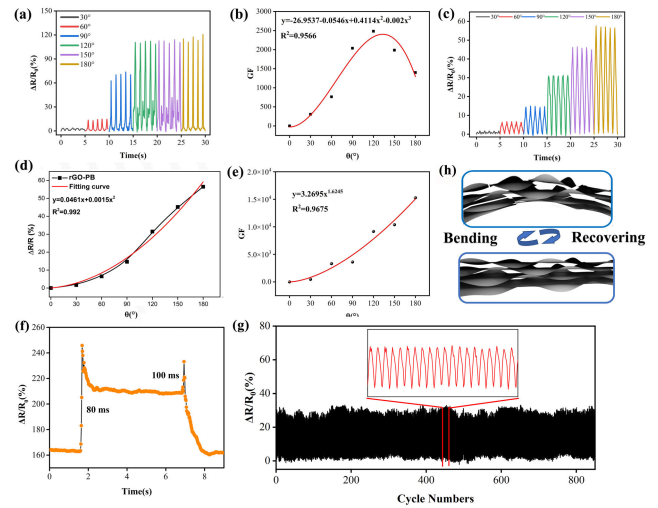

FIGURE 3. Sensing performance of pure rGO-Bs and rGO-PBs. (a) The resistance changes in graphene belts under different bending degrees; (b) GF of rGO-Bs; (c) resistance changes in rGO-PBs under different bending degrees; (d) fitting curve of resistance changes in the rGO-PB under different bending degrees; (e) GF of rGO-PBs; (f) response time of rGO-PB; (g) cyclic stability of rGO-PB; (h) deform sensing mechanism of rGO-PBs during bending.

radius of curvature, I represents the arc length, and c represents the chord length.

The GF curve of the rGO-Bs is shown in Figure 3(b). The sensitivity fitting curve of the pure rGO-Bs first increased, and then decreased, as shown in Figure 3(b). In detail, the GF of the rGO-Bs gradually increased from 0° to 120° with the bending angle and reached the maximum value of 2500. From 120° to 180°, the GF value of the pure rGO-Bs decreased. And the fitting degree (R_2) of the curve reached about 95.6%. In addition, the bending resistance changes in the rGO-PBs are shown in Figure 3(c). The resistance changes increased with the bending degree from 0° to 180°. Compared to the pure rGO-Bs, the rGO-PBs still had sensing performance at large bending degrees. These sensing performances indicate the rGO-PBs possessed a larger sensing range. The GF curve of the rGO-PBs also increased with the bending angle, as shown in Figure 3(d). The GF value of the rGO-PBs was about 1.5×10^4 at a bending degree of 180°. In addition, the R_2 reached about 96.7%, which was also higher than that of the pure rGO-Bs. These results might be attributed to the larger deformation of the rGO-PBs. In order to comprehensive evaluation of the sensor performance, the response time and the cyclic stability of rGO-PB were also invested in Figure 3. The response time of rGO-PB was about 80 ms and the recovery time was about 100 ms during the bending process as shown in Figure 3f. The fast response time could endow real-time detection performance to rGO-PB sensors. In addition, the cyclic stability was also investigated. As shown in Figure 3g, the rGO-PB was repeatedly and rapidly bent to 180° more than 800 times. During the bending tests, the resistance changes of rGO-PB were relatively stable, showing excellent durability as the inset of Figure 3g

demonstrated. The stable resistance changes indicated the inner structure of rGO-PB experienced steady deformation.

The sensing mechanism of rGO-PBs is described in this section. As shown in Figure 3(h), the rGO-PBs had many irregular inner pores in a normal state. These porous structures are the foundation for sensing and facilitate sensing with external stimuli. During the bending process, the graphene nano-sheets experienced slipping and dislocation in the inner structure. These slipping and dislocations form cracks in the pores, which directly led to a resistance increase. Moreover, these inner structure changes were enhanced with a gradual increase in the bending angle. Thus, the resistance changes increased with the bending degrees. When they returned to a normal state, these graphene nano-sheets recovered to their original state. Meanwhile, resistance also returned to a normal state. These inner structural changes would satisfy the requirements of deformation sensors.

Due to its excellent deformation sensing performance, a prepared rGO-PB was used as a wearable sensor. Flexible PDMS was used as a protective and insulated shell around the rGO-PBs. The morphology of the rGO-PB sensor was also observed. A digital image of the rGO-PB sensor is shown in Figure 4(a). The outside and protective shell is transparent, and the internal rGO-PB is black. A partially enlarged image of the rGO-PB sensor also displays the inner structure. The rGO-PB was in the middle part, and the PDMS film was positioned in the outside part. The cross-section image of the rGO-PB sensor shows the layer-upon-layer structure and porous structure as shown in Figure 4(a). During the encapsulation process, a small quantity of PDMS solution penetrated into the porous structure, and the pores between the faces became smaller. These results led to a certain improvement in the mechanical properties of the porous structure and enhanced the wearability of this flexible sensor. The resistance changes in the rGO-PB sensor during the stretching process are demonstrated in Figure 4(b). The elongation of the rGO-PB was larger than that of the pure rGO-Bs. These results indicate that the rGO-PB sensor had excellent flexibility due to its inner porous structure. PDMS not only
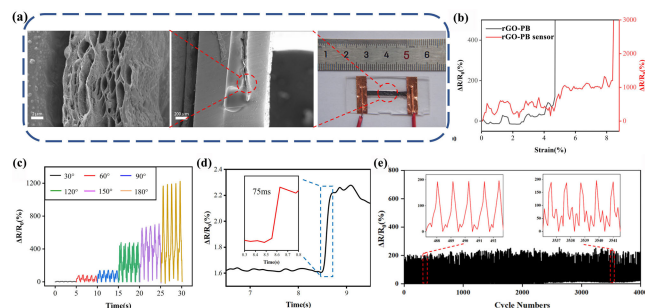
encapsulated the outside of the porous belts, but also infiltrated the inner pores. And this physical bonding improved its mechanical properties and also hindered the peeling and fracturing of the graphene layers. Thus, PDMS endowed the rGO-PB with excellent mechanical properties and a wider detection range for use as a wearable sensor.

The rGO-PB sensor was bent to different bending degrees as shown in Figure 4(c). With the increasing bending degrees, the rGO-PB sensor demonstrated a stepped increase. And the resistance also showed accuracy and stability in detecting different bending degrees. This result was according to the sensing performance of rGO-PB. In order to determine the response time, the encapsulated sensor was rapidly bent to 90°. The response time of the rGO-PB sensor was about 75 ms, as shown in Figure 4(d). As shown in Figure S6, the response time is similar to those of the previously reported Ag nanowire [53] and graphene woven fabric strain sensors [25]. This fast response time is superior to those of the previously reported wearable sensors, such as graphene-based fiber [23], film [38], [54], and aerogel sensors [55]. This fast response time may contribute to monitoring human motion, achieving real-time monitoring and converting complex signals into electrical signals. The cyclic stability of rGO-PB sensor was also measured. As shown in Figure 4(e), resistance changes in the rGO-PB sensor were measured at a bending angle of 90° after a test with 4,000 cycles. During the bending cycle process, the resistance changes in the rGO-PB sensor remained almost constant, demonstrating excellent stability. In addition, the resistance change curve in the initial state was smoother than that of at the end of the bending cycle test, as Figure 4(e) shows. At the beginning of the cyclic test, the $\Delta R/R_0$ resistance was about 190%. After 4,000 cycles, the resistance amplitude was about 185%. These differences indicate that the internal structural changes are tending toward stability during bending process. The rGO-PB sensor still had the same sensitivity even after the cyclic test. These results indicated the stability of the inner structure. Moreover, the deformed laminar structure recovered well during the cyclic bending test. These results prove that this sensor has good reliability and durability during bending cycles. As can be seen from the above results, the prepared rGO-PB sensor demonstrated a low detection limit, long durability, and fast response time. These performances indicate that rGO-PB sensors have promising applications as wearable sensors and could be used for detection in various fields.

C. APPLICATION OF RGO-PB SENOR

The prepared rGO-PB sensor had excellent durability, a wide bending range, and detection accuracy, enabling it to be used as a prototype of the wearable device. Thus, the rGO-PB sensor was installed on a person's skin for detecting and recognizing human motions. The rGO-PB sensor was first mounted on a joint to monitor the bending and stretching of their finger. Figure 5(a) shows the resistance variation in the rGO-PB sensor mounted on the finger at different

FIGURE 4. Performance of rGO-PB sensor. (a) Morphology of rGO-PB sensor; (b) the resistance changes in rGO-PB sensor during the drawing process; (c) the resistance changes in rGO-PB sensor under different bending degrees; (d) the response time of rGO-PB sensor; (e) the resistance changes in rGO-PB sensor after a test with 4000 cycles.
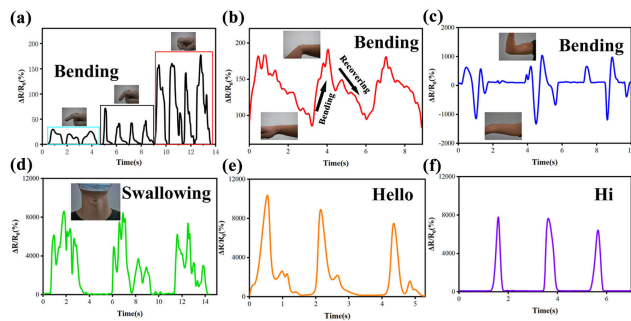
FIGURE 5. Wearable rGO-PB sensor used to detect and identify human motions. (a) The resistance changes in rGO-PB sensor in detecting the different motions of a finger; (b) and (c) the resistance change curves of rGO-PB sensor in detecting the motions of a wrist and upper arm; (d) the resistance change curve of rGO-PB sensor in detecting of swallowing; (e) and (f) the resistance change curves of rGO-PB sensor in detecting voice and identifying simple words.

bending angles. The resistance changes in the rGO-PB sensor increased with the bending degree of the finger, indicating excellent accuracy and stability. Then, the rGO-PB sensor was mounted on the person's wrist to detect the bending and stretching movements, as shown in Figure 5(b). The resistance curves demonstrate the bending and stretching of the wrist. As Figure 5(b) shows, the resistance change curve had some fluctuations, meaning that the wrist muscles' movements are complex during the bending process. In addition, the prepared rGO-PB sensor was installed on the upper arm muscle to detect motion. Interestingly, the resistance increased at the beginning, then decreased rapidly, and returned to a normal state as shown in Figure 5(c). These results were caused by complex movements of the upper arm muscles. These results also demonstrate that the rGO-PB sensor had outstanding accuracy in detecting complex movements. The above results show that the rGO-PB showed different responses and good stability in detecting flexion-relaxation movements. These results validate the possibility of rGO-PB sensors being a prototype for wearable devices.

Moreover, the prepared sensor was installed on a person's throat to detect the vibration of the laryngeal muscles. As shown in Figure 5(d), the rGO-PB sensor could monitor and identify swallowing actions. The test results show that the resistance signal changed with the vibration of the throat muscles. Furthermore, the rGO-PB sensor could detect muscle motion and recognize pronunciation and some simple words. As shown in Figure 5(e) and (f), the repetition of different words, such as "Hello" and "Hi", could be detected and identified. The accuracy and precision of detecting pronunciation demonstrate a promising application in helping persons with throat injuries. The results showed that the rGO-PB sensor could accurately monitor the changes in small vibrations. The tests on the joint and muscle vibrations showed that the prepared sensors would have helpful applications in monitoring all kinds of human movements. The excellent performance of rGO-PB sensors supports their use as wearable electronic devices.

IV. CONCLUSION

In conclusion, we propose a versatile and simple method for preparing highly sensitive, porous graphene belts (rGO-PBs). The prepared rGO-PBs had porous inner structures and excellent flexibility. The rGO-PBs had outstanding sensing performance in detecting bending angles. The formed rGO-PB sensor also demonstrated excellent accuracy, a fast response time (75ms), stability (4000 cycles), and good signal conversion. Wearable rGO-PBs sensors could detect and identify the different movements of the human body, such as the finger, wrist, and arm. More importantly, this wearable sensor could identify the vibration signal response of the throat and identify sample words. This low-cost fabrication method and the outstanding sensing performance of these rGO-PBs indicate great potential for future wearable electronics.

APPENDIX

Supplementary Materials: The following supplementary materials can be downloaded online. Figure S1: Digital image of neat pure rGO-Bs; Figure S2: XRD patterns of the prepared rGO-PBs; Figure S3: FTIR spectra of the prepared samples; Figure S4: XPS spectra of rGO-Bs; Figure S5: SEM image of composited GO-F at SEM image of composited GO-F; Figure S6: Comparison of the response time of the prepared rGO-PBs sensor in this work with some previously reported sensors.

INFORMED CONSENT

All subjects gave their informed consent for inclusion before they participated in the study. The study was conducted in accordance with the Declaration of Helsinki, and the protocol was approved by the Ethics Committee of Zhejiang SCI-Tech University.

REFERENCES

[1] P. Miao, J. Wang, C. Zhang, M. Sun, S. Cheng, and H. Liu, "Graphene nanostructure-based tactile sensors for electronic skin applications," *Nano-Micro Lett.*, vol. 11, no. 1, p. 37, Sep. 2019.

[2] A. F. Carvalho, B. Kulyk, A. J. S. Fernandes, E. Fortunato, and F. M. Costa, "A review on the applications of graphene in mechanical transduction," *Adv. Mater.*, vol. 34, no. 8, p. 55, Feb. 2022.

[3] Y. Qiao, X. Li, T. Hirtz, G. Deng, Y. Wei, M. Li, S. Ji, Q. Wu, J. Jian, F. Wu, and Y. Shen, "Graphene-based wearable sensors," *Nanoscale*, vol. 11, pp. 18923–18945, Nov. 2019.

[4] M. J. Allen, V. C. Tung, and R. B. Kaner, "Honeycomb carbon: A review of graphene," *Chem. Rev.*, vol. 110, no. 1, pp. 132–145, Jan. 2010.

[5] J. Ryu, J. Kim, J. Oh, S. Lim, J. Y. Sim, J. S. Jeon, K. No, S. Park, and S. Hong, "Intrinsically stretchable multi-functional fiber with energy harvesting and strain sensing capability," *Nano Energy*, vol. 55, pp. 348–353, Jan. 2019.

[6] R. Wu, L. Ma, A. Patil, Z. Meng, S. Liu, C. Hou, Y. Zhang, W. Yu, W. Guo, and X. Y. Liu, "Graphene decorated carbonized cellulose fabric for physiological signal monitoring and energy harvesting," *J. Mater. Chem. A*, vol. 8, no. 25, pp. 12665–12673, Jun. 2020.

[7] Y.-F. Yang, L.-Q. Tao, Y. Pang, H. Tian, Z.-Y. Ju, X.-M. Wu, Y. Yang, and T.-L. Ren, "An ultrasensitive strain sensor with a wide strain range based on graphene armour scales," *Nanoscale*, vol. 10, no. 24, pp. 11524–11530, 2018.

[8] Q. B. Zheng, J. H. Lee, X. Shen, X. D. Chen, and J. K. Kim, "Graphene-based wearable piezoresistive physical sensors," *Mater. Today*, vol. 39, p. 148, Oct. 2020.

[9] S.-N. Li, X.-F. He, Z.-F. Zeng, B. Jiang, Q. Wu, L.-X. Gong, Y. Li, J. Bae, S. Wang, and L.-C. Tang, "Mechanically ductile, ionically conductive and low-temperature tolerant hydrogel enabled by high-concentration saline towards flexible strain sensor," *Nano Energy*, vol. 103, Dec. 2022, Art. no. 107789.

[10] J. Han, J. Lee, J. Lee, and J. Yeo, "Highly stretchable and reliable, transparent and conductive entangled graphene mesh networks," *Adv. Mater.*, vol. 30, no. 3, Jan. 2018, Art. no. 1704626.

[11] T. Q. Trung and N. Lee, "Flexible and stretchable physical sensor integrated platforms for wearable human–activity monitoringand personal healthcare," *Adv. Mater.*, vol. 28, no. 22, pp. 4338–4372, Jun. 2016.

[12] S. Liu, J. Zhang, Y. Zhang, and R. Zhu, "A wearable motion capture device able to detect dynamic motion of human limbs," *Nature Commun.*, vol. 11, no. 1, p. 5615, Nov. 2020.

[13] Q. Chen, J. Yang, B. Chen, J. Feng, S. Xiao, Q. Yue, X. Zhang, and T. Wang, "Wearable pressure sensors with capacitive response over a wide dynamic range," *ACS Appl. Mater. Interfaces*, vol. 14, no. 39, pp. 44642–44651, Oct. 2022.

[14] S.-N. Li, Z.-R. Yu, B.-F. Guo, K.-Y. Guo, Y. Li, L.-X. Gong, L. Zhao, J. Bae, and L.-C. Tang, "Environmentally stable, mechanically flexible, self-adhesive, and electrically conductive Ti_3C_2TX MXene hydrogels for wide-temperature strain sensing," *Nano Energy*, vol. 90, Dec. 2021, Art. no. 106502.

[15] Q.-Y. Ni, X.-F. He, J.-L. Zhou, Y.-Q. Yang, Z.-F. Zeng, P.-F. Mao, Y.-H. Luo, J.-M. Xu, B. Jiang, Q. Wu, B. Wang, Y.-Q. Qin, L.-X. Gong, L.-C. Tang, and S.-N. Li, "Mechanical tough and stretchable quaternized cellulose nanofibrils/MXene conductive hydrogel for flexible strain sensor with multi-scale monitoring," *J. Mater. Sci. Technol.*, vol. 191, pp. 181–191, Aug. 2024.

[16] A. I. Faisal, S. Majumder, T. Mondal, D. Cowan, S. Naseh, and M. J. Deen, "Monitoring methods of human body joints: State-of-the-art and research challenges," *Sensors*, vol. 19, no. 11, p. 2629, Jun. 2019.

[17] Y. Zhang, P. He, M. Luo, X. Xu, G. Dai, and J. Yang, "Highly stretchable polymer/silver nanowires composite sensor for human health monitoring," *Nano Res.*, vol. 13, no. 4, pp. 919–926, Apr. 2020.

[18] M. A. Butt, N. L. Kazanskiy, and S. N. Khonina, "Revolution in flexible wearable electronics for temperature and pressure monitoring—A review," *Electronics*, vol. 11, no. 5, p. 716, Feb. 2022.

[19] L.-Y. Lv, C.-F. Cao, Y.-X. Qu, G.-D. Zhang, L. Zhao, K. Cao, P. Song, and L.-C. Tang, "Smart fire-warning materials and sensors: Design principle, performances, and applications," *Mater. Sci. Eng., R, Rep.*, vol. 150, Aug. 2022, Art. no. 100690.

[20] J. Zhang, R. Song, X. Zhao, R. Fang, B. Zhang, W. Qian, J. Zhang, C. Liu, and D. He, "Flexible graphene-assembled film-based antenna for wireless wearable sensor with miniaturized size and high sensitivity," *ACS Omega*, vol. 5, no. 22, pp. 12937–12943, Jun. 2020.

[21] T. Huang, S. Yang, P. He, J. Sun, S. Zhang, D. Li, Y. Meng, J. Zhou, H. Tang, J. Liang, G. Ding, and X. Xie, "Phase-separation-induced PVDF/graphene coating on fabrics toward flexible piezoelectric sensors," *ACS Appl. Mater. Interface*, vol. 10, no. 36, pp. 30732–30740, Sep. 2018.

[22] Z. Yang, Y. Pang, X.-L. Han, Y. Yang, J. Ling, M. Jian, Y. Zhang, Y. Yang, and T.-L. Ren, "Graphene textile strain sensor with negative resistance variation for human motion detection," *ACS Nano*, vol. 12, no. 9, pp. 9134–9141, Sep. 2018.

[23] T. Huang, P. He, R. Wang, S. Yang, J. Sun, X. Xie, and G. Ding, "Porous fibers composed of polymer nanoball decorated graphene for wearable and highly sensitive strain sensors," *Adv. Funct. Mater.*, vol. 29, no. 45, p. 9, Nov. 2019.

[24] M. Alahmar, B. Younes, and I. Alghoraibi, "Modification of cotton yarns utilizing graphene ink to functionalized as conductivity," *J. Textile Inst.*, pp. 1–12, Feb. 2024, doi: 10.1080/00405000.2024.2308938.

[25] X. Liu, C. Tang, X. Du, S. Xiong, S. Xi, Y. Liu, X. Shen, Q. Zheng, Z. Wang, Y. Wu, A. Horner, and J.-K. Kim, "A highly sensitive graphene woven fabric strain sensor for wearable wireless musical instruments," *Mater. Horizons*, vol. 4, no. 3, pp. 477–486, 2017.

[26] Q. Chen, J. Shen, D. Estevez, Y. Chen, Z. Zhu, J. Yin, and F. Qin, "Ultraprecise 3D printed graphene aerogel microlattices on tape for micro sensors and E-skin," *Adv. Funct. Mater.*, vol. 33, no. 33, Apr. 2023, Art. no. 2302545.

[27] Y. Li, T. He, L. Shi, R. Wang, and J. Sun, "Strain sensor with both a wide sensing range and high sensitivity based on braided graphene belts," *ACS Appl. Mater. Interface*, vol. 12, no. 15, pp. 17691–17698, Apr. 2020.

[28] P. Kumar, F. Shahzad, S. Yu, S. M. Hong, Y.-H. Kim, and C. M. Koo, "Large-area reduced graphene oxide thin film with excellent thermal conductivity and electromagnetic interference shielding effectiveness," *Carbon*, vol. 94, pp. 494–500, Nov. 2015.

[29] Y. Zhang, Q. Wan, and N. Yang, "Recent advances of porous graphene: Synthesis, functionalization, and electrochemical applications," *Small*, vol. 15, no. 48, Oct. 2019, Art. no. 1903780.

[30] A. C. Lokhande, I. A. Qattan, C. D. Lokhande, and S. P. Patole, "Holey graphene: An emerging versatile material," *J. Mater. Chem. A*, vol. 8, no. 3, pp. 918–977, Jan. 2020.

[31] L. Jiang and Z. Fan, "Design of advanced porous graphene materials: From graphene nanomesh to 3D architectures," *Nanoscale*, vol. 6, no. 4, pp. 1922–1945, 2014.

[32] C. Tang, H. Wang, H. Wang, Q. Zhang, G. Tian, J. Nie, and F. Wei, "Spatially confined hybridization of nanometer-sized NiFe hydroxides into nitrogen-doped graphene frameworks leading to superior oxygen evolution reactivity," *Adv. Mater.*, vol. 27, no. 30, pp. 4516–4522, Jun. 2015.

[33] Y. Pang, J. Jian, T. Tu, Z. Yang, J. Ling, Y. Li, X. Wang, Y. Qiao, H. Tian, Y. Yang, and T.-L. Ren, "Wearable humidity sensor based on porous graphene network for respiration monitoring," *Biosensors Bioelectron.*, vol. 116, pp. 123–129, Sep. 2018.

[34] L. Lu, J. T. M. De Hosson, and Y. Pei, "Three-dimensional micron-porous graphene foams for lightweight current collectors of lithium-sulfur batteries," *Carbon*, vol. 144, pp. 713–723, Apr. 2019.

[35] R. B. Ambade, K. H. Lee, D. J. Kang, and T. H. Han, "Advances in porous graphene and scalable wet-spinning fiber assembly," *Accounts Mater. Res.*, vol. 4, no. 5, pp. 389–402, May 2023.

[36] K.-Y. Chen, Y.-T. Xu, Y. Zhao, J.-K. Li, X.-P. Wang, and L.-T. Qu, "Recent progress in graphene-based wearable piezoresistive sensors: From 1D to 3D device geometries," *Nano Mater. Sci.*, vol. 5, no. 3, pp. 247–264, Sep. 2023.

[37] L. Yang, B. Feng, Y. Zhang, X. Li, L. Zhang, X. Chen, J. Nie, H. Wen, J. Tian, J. Jian, J. Huang, D. Zhu, A. Zhang, X. Tong, and L. Wen, "Single wire capacitive wireless power transfer system for wearable biomedical sensors based on flexible graphene film material," *IEEE Trans. Biomed. Circuits Syst.*, vol. 16, no. 6, pp. 1337–1347, Dec. 2022.

[38] J. Jia, G. Huang, J. Deng, and K. Pan, "Skin-inspired flexible and high-sensitivity pressure sensors based on rGO films with continuous-gradient wrinkles," *Nanoscale*, vol. 11, no. 10, pp. 4258–4266, Mar. 2019.

[39] L. Sheng, Y. Liang, L. Jiang, Q. Wang, T. Wei, L. Qu, and Z. Fan, "Bubble-decorated honeycomb-like graphene film as ultrahigh sensitivity pressure sensors," *Adv. Funct. Mater.*, vol. 25, no. 41, pp. 6545–6551, Nov. 2015.

[40] Z. Wang, P. Li, R. Song, W. Qian, H. Zhou, Q. Wang, Y. Wang, X. Zeng, L. Ren, S. Yan, S. Mu, and D. He, "High conductive graphene assembled films with porous micro-structure for freestanding and ultra-low power strain sensors," *Sci. Bull.*, vol. 65, no. 16, pp. 1363–1370, Aug. 2020.

[41] D. Lai, X. Chen, and Y. Wang, "Controllable fabrication of elastomeric and porous graphene films with superior foldable behavior and excellent electromagnetic interference shielding performance," *Carbon*, vol. 158, pp. 728–737, Mar. 2020.

[42] H. Chen, Z. Chen, M. Mao, Y. Wu, F. Yang, L. Gong, L. Zhao, C. Cao, P. Song, J. Gao, G. Zhang, Y. Shi, K. Cao, and L. Tang, "Self-adhesive polydimethylsiloxane foam materials decorated with MXene/cellulose nanofiber interconnected network for versatile functionalities," *Adv. Funct. Mater.*, vol. 33, no. 48, p. 12, Nov. 2023.

[43] F. Nie, Y. Gu, L. Zhao, L. Li, F. Shen, J. Song, J. Liu, G. Zhang, J. Gao, P. Song, Y. Shi, and L. Tang, "Construction of conductive polymer coatings onto flexible PDMS foam composites with exceptional mechanical robustness for sensitive strain sensing applications," *Adv. Sensor Res.*, vol. 3, no. 4, Apr. 2024, Art. no. 2300140.

[44] W. Yu, L. Sisi, Y. Haiyan, and L. Jie, "Progress in the functional modification of graphene/graphene oxide: A review," *RSC Adv.*, vol. 10, no. 26, pp. 15328–15345, Apr. 2020.

[45] P. Xue, C. Chen, and D. Diao, "Ultra-sensitive flexible strain sensor based on graphene nanocrystallite carbon film with wrinkle structures," *Carbon*, vol. 147, pp. 227–235, Jun. 2019.

[46] A. S. Sai Pavan and S. R. Ramanan, "A study on corrosion resistant graphene films on low alloy steel," *Appl. Nanoscience*, vol. 6, no. 8, pp. 1175–1181, Nov. 2016.

[47] L. Stobinski, B. Lesiak, A. Malolepszy, M. Mazurkiewicz, B. Mierzwa, J. Zemek, P. Jiricek, and I. Bieloshapka, "Graphene oxide and reduced graphene oxide studied by the XRD, TEM and electron spectroscopy methods," *J. Electron Spectrosc. Rel. Phenomena*, vol. 195, pp. 145–154, Aug. 2014.

[48] H.-H. Huang, K. K. H. De Silva, G. R. A. Kumara, and M. Yoshimura, "Structural evolution of hydrothermally derived reduced graphene oxide," *Sci. Rep.*, vol. 8, no. 1, p. 6849, May 2018.

[49] F. T. Johra and W.-G. Jung, "Hydrothermally reduced graphene oxide as a supercapacitor," *Appl. Surf. Sci.*, vol. 357, pp. 1911–1914, Dec. 2015.

[50] S. Jalili-Firoozinezhad, M. H. M. Moghadam, M. H. Ghanian, M. K. Ashtiani, H. Alimadadi, H. Baharvand, I. Martin, and A. Scherberich, "Polycaprolactone-templated reduced-graphene oxide liquid crystal nanofibers towards biomedical applications," *RSC Adv.*, vol. 7, no. 63, pp. 39628–39634, 2017.

[51] J. Zhu, Q. Li, Y. Che, X. Liu, C. Dong, X. Chen, and C. Wang, "Effect of Na_2CO_3 on the microstructure and macroscopic properties and mechanism analysis of PVA/CMC composite film," *Polymers*, vol. 12, no. 2, p. 453, Feb. 2020.

[52] X. Qi, H. Ha, B. Hwang, and S. Lim, "Printability of the screen-printed strain sensor with carbon black/silver paste for sensitive wearable electronics," *Appl. Sci.*, vol. 10, no. 19, p. 6983, Oct. 2020.

[53] X. Wang, Y. Zhang, X. Zhang, Z. Huo, X. Li, M. Que, Z. Peng, H. Wang, and C. Pan, "A highly stretchable transparent self-powered triboelectric tactile sensor with metallized nanofibers for wearable electronics," *Adv. Mater.*, vol. 30, no. 12, p. 8, Mar. 2018.

[54] Y. Wang, J. Hao, Z. Huang, G. Zheng, K. Dai, C. Liu, and C. Shen, "Flexible electrically resistive-type strain sensors based on reduced graphene oxide-decorated electrospun polymer fibrous mats for human motion monitoring," *Carbon*, vol. 126, pp. 360–371, Jan. 2018.

[55] Y. Ma, Y. Yue, H. Zhang, F. Cheng, W. Zhao, J. Rao, S. Luo, J. Wang, X. Jiang, Z. Liu, N. Liu, and Y. Gao, "3D synergistical MXene/reduced graphene oxide aerogel for a piezoresistive sensor," *ACS Nano*, vol. 12, no. 4, pp. 3209–3216, Apr. 2018.

SHUAI LIU was born in Chuzhou, Anhui, China, in 1998. He received the B.S. degree in textile engineering from Zhongyuan University of Technology, in 2020. He is currently pursuing the master's degree with Zhejiang Sci-Tech University, China, with a focus on the graphene-based materials and smart wearable sensors.

ZHAOFA ZHANG was born in Shandong, China, in 1991. He received the B.S. and Ph.D. degrees in textile engineering from Soochow University, Suzhou, China, in 2014 and 2019, respectively. He has been a Lecturer with the College of Textile Science and Engineering, Zhejiang Sci-Tech University, since 2020. He has authored more than ten articles. His research interests include the synthesis of graphene-based materials; functional fibers, yarns, and textiles; toward their applications in high performance, flexible, and stretchable electronics; and smart wearable systems.

● ● ●